View metadata, citation and similar papers at core.ac.uk
brought to you by CORE
provided by Apollo

Greenhouse Gas and Noxious Emissions from Dual Fuel Diesel and Natural Gas Heavy Goods Vehicles

Marc E.J. Stettler[1,2]*, William J.B. Midgley[1], Jacob J. Swanson[3], David Cebon[1], Adam M. Boies[1]

[1]Centre for Sustainable Road Freight, Department of Engineering, University of Cambridge, Cambridge, CB2 1PZ, UK.

[2]Centre for Transport Studies, Department of Civil and Environmental Engineering, Imperial College London, London SW7 2AZ, UK.

[3]Minnesota State University, Mankato, Mankato, Minnesota, 56001, USA.

*Corresponding author: Centre for Transport Studies, Department of Civil and Environmental Engineering, Imperial College London, London SW7 2AZ, UK. Tel: +44 (0) 207 594 2094. Fax: +44 (0) 207 594 6102. Email: m.stettler@imperial.ac.uk

Abstract

Dual fuel diesel and natural gas heavy goods vehicles (HGVs) operate on a combination of the two fuels simultaneously. By substituting diesel for natural gas, vehicle operators can benefit from reduced fuel costs and as natural gas has a lower CO_2 intensity compared to diesel, dual fuel HGVs have the potential to reduce greenhouse gas (GHG) emissions from the freight sector. In this study, energy consumption, greenhouse gas and noxious emissions for five after-market dual fuel configurations of two vehicle platforms are compared relative to their diesel-only baseline values over transient and steady state testing. Over a transient cycle, CO_2 emissions are reduced by up to 9% however methane (CH_4) emissions due to incomplete combustion lead to CO_2e emissions that are 50-127% higher than the equivalent diesel vehicle. Oxidation catalysts evaluated on the vehicles at steady state reduced CH_4 emissions by at most 15% at exhaust gas temperatures representative of transient conditions. This study highlights that control of CH_4 emissions and improved control of in-cylinder CH_4 combustion are required to reduce total GHG emissions of dual fuel HGVs relative to diesel vehicles.

1 Introduction

1.1 Context

Globally, road freight transport is responsible for around a quarter of transport energy use[1]. In the UK, heavy goods vehicles (HGVs) involved in freight movements account for 22% and 23% of road transport energy use[2] and greenhouse gas (GHG) emissions[3] respectively. Long haul and regional duty cycles account for approximately 70% of UK HGV CO_2 emissions and the substitution of natural gas (NG) for diesel has the potential to reduce HGV CO_2 emissions due to the lower CO_2 intensity of methane compared to diesel[4]. In 2012, the UK Technology Strategy Board and the Office for Low Emission Vehicles provided £11.3m (~$17.5m) to trials of 362 diesel-NG dual fuel trucks, using five different dual fuel systems. Four out of five of these systems are aftermarket conversions, while one is supplied by an original equipment manufacturer (OEM)[5]. In 2013, the European Commission provided €14.3m (~$15.6m) to the trial of 100 LNG HGVs, including dual fuel vehicles[6]. In the US, the Environmental Protection Agency has certified one diesel-NG conversion system for new engines, which grants exemption from the Clean Air Act tampering prohibition, and a number of other dual fuel systems for intermediate age engines[7].

The use of NG as a transport fuel is at least partially motivated by the potential to reduce CO_2 emissions. The primary component of NG is methane (CH_4). As CH_4 has a higher ratio of hydrogen to carbon atoms (4:1) than diesel (~2:1), less CO_2 is emitted per unit of chemical energy released by combustion. A dual fuel engine is a conventional compression ignition diesel engine in which a significant proportion of the energy released by combustion is derived from the combustion of a gaseous fuel, such as NG[8]. All of the dual fuel systems installed on vehicles residing the UK operate by injecting NG into the intake air prior to the intake valves so that a NG-air mixture is drawn into the combustion chamber[5,9–12]. This NG-air charge is then ignited by an injection of diesel at the end of the compression stroke, which has a shorter ignition delay than the NG[8]. This dual fuel concept differs from systems that employ high-pressure direct injection (HPDI) of NG into the combustion chamber[13].

Dual fuel engines offer an attractive alternative to other engine technologies due to the (i) higher thermal efficiency relative to spark-ignited engines, (ii) flexible fuel capability with the option to operate solely on diesel when gaseous fuel is not available, (iii) reduced fuel costs, and (iv) reductions in emissions of CO_2 and other engine exhaust components[4,14]. Previous studies of dual fuel engine emissions have focussed on engine dynamometer testing, rather than full vehicle emissions testing. These studies have shown significant changes to emissions when compared to conventional diesel engines[8,14–21]. Dual fuel engine emissions depend on a number of parameters including the engine speed, engine load, the composition

and quantity of primary gaseous fuel, the quantity of pilot diesel, the temperature of the intake primary fuel and air mixture, the pilot injection timing and stratification of the gaseous fuel and air mixture[16,21–23]. In previous studies, dual fuel combustion with NG as the primary fuel led to reduced emissions of oxides of nitrogen (NO_x) but increased emissions of carbon monoxide (CO) and unburnt hydrocarbons (HC)[14–21]. The majority of the unburnt hydrocarbon emissions from a NG dual fuel engines is CH_4 and the magnitude of these emissions depended strongly on the concentration of the gaseous fuel in the cylinder[14,18]. Using a global warming potential (GWP) of 25 for CH_4, Besch et al.[18] showed that while CO_2 emissions were reduced by 3-8% for three dual fuel engines relative to diesel operation over the heavy duty engine Federal Test Procedure, emissions of CH_4 led to 18-129% increases in CO_2e emissions.

Previous smoke opacity measurements have shown that diesel and NG dual fuel combustion has the potential to reduce smoke emissions[19,20,24]. Graves et al.[25] characterised the morphology and volatility of particles emitted by an HPDI dual fuel engine, however this is a distinctly different dual fuel concept from that employed by the systems currently in use and evaluated in this study.

1.2 Overview

This paper presents an evaluation of transient and steady state energy use, greenhouse gas, nitrous oxides, carbon monoxide and particulate matter (PM) emissions of five vehicle configurations of two dual fuel aftermarket conversion systems that account for the majority (~60%) of the 362 trialled dual fuel vehicles in the UK[5]. In contrast to previous studies that have tested engines installed on engine dynamometers[21], this study tests in-use vehicles with emissions control devices on a chassis dynamometer to quantify dual fuel HGV emissions factors for subsequent use in environmental impact assessments and provide emissions metrics that are relevant to policy makers and logistics fleet operators. Furthermore, this paper highlights areas for technology development. Due to commercial sensitivities, the vehicle owners and the dual fuel conversion suppliers have not been disclosed.

2 Materials and methods

2.1 Outline of study

The vehicle configurations and specifications of the original vehicle platforms are summarised in Table 1. This study's authors did not modify or attempt to control the performance of the dual fuel systems or fuelling strategies. On both vehicles where methane

oxidation catalysts are present, these were installed upstream of the OEM selective catalytic reduction (SCR) unit by the dual fuel conversion suppliers. The dosing of aqueous urea solution in the SCR systems on both vehicles was not altered and neither vehicle was fitted with a diesel particulate filter. Configurations A0 (4×2 tractor) and B0 (6×2 tractor) are taken as baseline tests, while A1 and B1 are the most common diesel-NG dual fuel vehicle configurations for suppliers A and B respectively. The configuration in A2 and A4 is unique for this study and is not a standard option offered by supplier A; it was tested to evaluate the impact of an oxidation catalyst on performance and emissions. This oxidation catalyst was a prototype design that was installed immediately before these emissions tests were conducted. In contrast, the oxidation catalyst on vehicle B had been installed on the vehicle for approximately 500,000 km and is therefore is representative of catalysts in operation.

Transient cycle and steady state vehicle emissions testing was conducted on a 1.22 m (42 in.) single roll chassis dynamometer capable of simulating 20 tonnes of inertia (Millbrook Proving Ground Ltd, Bedford, MK45 2JQ, UK). Further experimental details including fuel properties and uncertainty analyses are shown in the Supporting Information.

Table 1: Test vehicle specifications and list of transient test parameters.

Base vehicle	Ref.	After-treatment	Fuel	Hot/cold start
EURO V 4×2 tractor	A0	SCR	Diesel	Hot
Max power: 228 kW	A1	SCR	Dual fuel	Hot
Max torque: 1275 Nm	A2	SCR & Oxi cat	Dual fuel	Hot
Engine displacement: 9.2 L	A3	SCR	Dual fuel	Cold
Compression ratio: 17.4	A4	SCR & Oxi cat	Dual fuel	Cold
Bore/ Stroke: 118/140 mm				
Wheelbase: 3.6 m				
EURO V 6×2 tractor	B0	SCR & Oxi cat	Diesel	Hot
Max power: 295 kW	B1	SCR & Oxi cat	Dual fuel	Hot
Max torque: 2000 Nm	B2	SCR & Oxi cat	Dual fuel	Cold
Engine displacement: 11.97 L				
Compression ratio: 18.5				
Bore/ Stroke: 128/155 mm				
Wheelbase: 3.9 m				

2.2 Test cycles

Transient cycle emissions were obtained over the vehicle version of the European Transient Cycle, developed by the FIGE Institute[26]. The FIGE cycle has three distinct phases, representing urban (U), rural (R) and motorway (M) driving. Hot start tests followed a consistent engine warm up procedure, while cold start tests were conducted at 0°C after the vehicle had been soaked overnight. Steady state emissions testing on the chassis dynamometer was conducted to develop a map of engine emissions as a function of engine torque and speed (revolutions per minute, rpm) that would also be of further use in vehicle emissions models[27]. Engine speed and torque were systematically varied in ~200 rpm and ~200 Nm steps respectively. Each test point was held for at least two minutes, consistent with regulatory engine test cycles[28,29].

2.3 Instrumentation

The net flow rate of diesel supplied to the engines was measured using an FMS MK10 fuel flowmeter (JPS Engineering, UK), which recorded flow in 5 mL increments. The mass flow rate of NG delivered to the engines was measured by a Rotamass RCCS34 Coriolis flow meter (Yokogawa Electric Corporation, Japan) placed in line between the low pressure regulator and gas injectors of the dual fuel systems. This Coriolis flow meter was sized to minimise interference with dual fuel system by minimising pressure drop while maintaining accuracy; at a nominal flow rate of 22.5 kg/hour at 5 bar and 20°C, the pressure drop and accuracy were calculated to be 17 mbar and 1.1% respectively. The energy substitution ratio (ESR) is defined as the proportion of total energy supplied to the engine in the form of NG,

$$\text{ESR}\,[\%] = \frac{\dot{m}_{\text{NG,in}}\text{LCV}_{\text{NG}}}{\dot{m}_{\text{NG,in}}\text{LCV}_{\text{NG}} + \dot{m}_{\text{diesel,in}}\text{LCV}_{\text{diesel}}} \times 100\,, \quad (1)$$

where $\dot{m}_{\text{NG,in}}$ and $\dot{m}_{\text{diesel,in}}$ are the mass flow rates of NG and diesel supplied to the engine respectively, and LCV is the lower calorific value of the fuel.

Engine emissions and exhaust gas temperatures were measured at two locations in the exhaust; (i) post-turbo (PT), equivalent to an engine-out measurement, and (ii) at the tailpipe. A complete list of the emissions analysers and emissions species is included in the SI. Reported emissions factors have been calculated based on the modal 1 Hz data for transient and steady state testing. For CO_2, NO_x and CO, these emissions factors were within 1%, 1% and 7% of emissions factors calculated based on averaged bag measurements over the entire transient test cycle.

CH_4 emissions were measured at the post-turbo and tailpipe locations using Fourier Transform Infra-Red (FTIR) spectrometers (Multigas 2030 and 2030 HS respectively, MKS Instruments, MA, USA). CH_4 slip is reported as the ratio of the mass flow rate of exhausted CH_4, $\dot{m}_{\text{CH}_4,\text{tailpipe}}$, to the mass flow rate of CH_4 supplied to the engine in the NG, $\dot{m}_{\text{CH}_4,\text{in}}$,

$$\text{CH}_4\text{ slip}\,[\%] = \frac{\dot{m}_{\text{CH}_4,\text{tailpipe}}}{\dot{m}_{\text{CH}_4,\text{in}}} \times 100\%\,. \quad (2)$$

The effectiveness of oxidation catalysts in the vehicles' exhaust after-treatment systems was evaluated by comparing CH_4 concentrations at the post-turbo and tailpipe sampling points measured by the two FTIR instruments.

A DMS500 (Cambustion Ltd, UK) measured real-time particle size distributions at the tailpipe. PM and black carbon (BC) mass emissions were estimated using the integrated particle size distribution (IPSD) method[30,31]. The aggregate effective density, ρ_{eff}, as a function of mobility diameter, d_{p}, was calculated as

$$\rho_{\text{eff}} = \rho_0 \left(\frac{d_{\text{p}}}{d_{\text{pp}}}\right)^{D_{\text{m}}}, \quad (3)$$

where ρ_0 is the material density, d_{pp} is the primary particle diameter and D_{m} is the mass-mobility exponent with assumed values of 2 g/cm^3, 16 nm and 2.35 respectively[32]. For d_{p} less than 30 nm, an effective density of 1.46 g/cm^3 is assumed[32]. Total PM mass was

calculated by integrating over the entire size distribution (5-1000 nm), while for BC, a lognormal distribution was fitted to the accumulation mode. Reported particle number (PN) emissions factors are calculated by summing the product of the particle size distribution and a detection efficiency curve[33] fitted to data for condensation particle counters with detection efficiencies of 50% at 23 nm[34]. This enables comparison to measurements following the solid particle number measurement protocol developed through the Particle Measurement Programme (PMP)[35].

Total GHG emissions, as CO_2e were calculated by summing CO_2, CH_4, N_2O, NO_x, CO and BC emissions multiplied by their GWPs for a time horizon of 100 years. GWPs for CH_4 (34) and N_2O (298) are taken from the IPCC's Fifth Assessment Report (AR5) and include climate-carbon feedbacks [36]. All GWPs are included in the SI and we note that choosing a shorter time horizon (e.g. 20 years) would increase the importance of short-lived species (e.g. CH_4).

3 Results

3.1 Transient cycle energy consumption and emissions

Distance specific energy consumption and emissions factors over different phases of the FIGE cycle (U = urban, R = rural, M = motorway, C = combined) for the different vehicle configurations are shown in Table 2 and Table 3. This data is shown graphically in the SI. Distance specific energy consumption is generally highest during the urban phase, followed by the motorway and rural phases for all vehicle configurations. In general, dual fuel operation reduces energy efficiency and results in higher total energy consumption compared to the baseline diesel only tests (A0 and B0). For A1 and B1, combined energy consumption is 12% and 10% higher than the equivalent diesel tests. Previous studies have also shown that energy efficiency of dual fuel engines are reduced compared to diesel at low and intermediate engine loads, which is attributed to lower combustion efficiency of the lean NG-air charge mixture and higher rates of heat loss during combustion[21]. Over the four dual fuel tests with vehicle A, higher ESR during A1 and A3 compared to A2 and A4, indicate that the dual fuel system supplier may have updated their control software. Comparing A1 to A2, higher ESR is correlated with higher energy consumption yet lower CO_2 emissions. For vehicles A and B, the highest ESR is observed during the motorway phase and during this phase, the CO_2 emissions factor is lowest and the relative reduction compared to diesel is greatest at up to 11% and 13% for A1 and B1 respectively. For context, the fuel properties (shown in the SI)

indicate that complete combustion of NG would emit approximately 21% less CO_2 per unit of energy than diesel used in this study, assuming no change in energy efficiency. For the cold start tests, (A3, A4 and B2), distance specific energy consumption and emissions of CO_2 are generally greater than the equivalent hot start test. Both dual fuel conversion suppliers account for engine temperature in their control of the ESR; during the urban phase, when engine temperatures are cold, the ESR is significantly reduced relative to the same phase in hot start tests.

Table 2: Energy consumption, energy substitution ratio, CO_2 and CO_2e emissions factors from transient testing. U = urban, R = rural, M = motorway, C = combined phases of the FIGE cycle.

	Energy (MJ/km)				ESR (%)				CO_2 (g/km)				CO_2e (g/km)			
Ref.	U	R	M	C	U	R	M	C	U	R	M	C	U	R	M	C
A0	12.8	10.2	10.5	10.7	0	0	0	0	957	753	747	777	954	751	740	772
A1	13.7	11.1	12.3	12.0	37.6	45.9	58.3	50.9	923	686	662	705	1264	931	1055	1036
A2	12.5	10.4	11.6	11.3	31.0	37.1	51.4	43.4	920	708	663	714	1344	1013	1239	1168
A3	16.7	11.5	12.3	12.6	16.5	46.8	59.3	49.1	1175	711	676	753	1305	952	1083	1062
A4	13.1	12.1	12.6	12.5	5.4	37.3	48.7	40.0	1184	724	673	744	1269	1089	1352	1242
B0	14.6	10.1	11.0	11.2	0	0	0	0	1135	754	742	798	1129	758	748	801
B1	20.4	9.9	11.9	12.2	32.7	53.6	73.5	60.7	1156	692	649	730	2522	1408	1945	1817
B2	15.7	13.3	14.3	14.1	0.9	54.0	71.1	57.4	1443	703	650	751	1380	1550	2418	1977

CO_2 and CH_4 (shown in Table 3) dominated total CO_2e emissions and capture the first-order climate impacts of dual fuel relative to diesel. The combined cycle relative contribution of CH_4 normalised to the CO_2 contribution was between 40% for A3 and 150% for B2. CH_4 emissions factors are typically highest during the motorway phase, which is also the phase with highest ESR. For all dual fuel tests on both vehicles, CH_4 emissions led to increased CO_2e emissions relative to the diesel baseline tests. Comparing A1 to A0 and B1 to B0, dual fuel operation increased CO_2e emissions factors by 32%, 24%, 42% and 123%, 86%, 160% for the urban, rural and motorway phases respectively. Therefore, it is clear that CH_4 emissions outweigh potential reductions in CO_2 emissions that result from substituting diesel for NG. For A1, 8.4%, 6.5% and 8.1%, and for B1, 30.1%, 18.4% and 21.0% of CH_4 that is delivered to the engine is emitted to the atmosphere during the urban, rural and motorway phases respectively. These findings are in agreement with previous engine dynamometer testing of dual fuel retrofit systems, which also measured significant increases in CO_2e emissions due to CH_4 emissions[18]. The addition of an oxidation catalyst to A2 compared to A1 did not significantly reduce CH_4 emissions; indeed distance specific CH_4 emissions are

increased, which could be indicative of an altered fuelling strategy or that backpressure due to the oxidation catalyst may have had an adverse effect on in-cylinder combustion and therefore engine emissions performance. Oxidation catalyst effectiveness is discussed further in Section 3.3.

Table 3: NO_x, CH_4, PM and PN emissions from transient testing. U = urban, R = rural, M = motorway, C = combined phases of the FIGE cycle.

	NO_x (g/km)				CH_4 (g/km)				PM mass (mg/km)				PN ($\times 10^{14}$ #/km)			
Ref.	U	R	M	C	U	R	M	C	U	R	M	C	U	R	M	C
A0	7.8	4.4	4.0	4.6	0.0	0.0	0.0	0.0	54.5	26.8	19.5	26.8	1.66	0.84	0.72	0.89
A1	7.4	3.6	1.9	3.3	8.5	6.5	11.4	9.2	77.8	48.3	13.8	35.1	1.89	1.10	0.43	0.87
A2	10.2	4.4	2.0	4.0	11.5	8.3	16.5	12.8	89.0	54.5	24.6	44.2	2.31	1.47	0.79	1.24
A3	12.3	4.4	2.1	4.2	3.9	6.6	11.8	8.8	29.4	36.3	12.7	23.7	0.61	0.85	0.37	0.58
A4	14.3	5.3	2.6	4.8	2.3	10.5	19.8	14.4	76.2	33.6	13.8	27.7	2.12	0.93	0.51	0.83
B0	7.3	1.0	0.3	1.5	0.0	0.0	0.0	0.0	28.7	10.7	6.9	11.2	0.99	0.28	0.22	0.34
B1	2.4	0.9	2.3	1.8	38.9	18.9	35.6	29.7	40.4	13.9	8.5	14.7	1.38	0.31	0.25	0.42
B2	19.7	2.8	2.6	4.4	0.1	24.7	45.8	33.0	13.0	6.3	5.1	6.3	0.38	0.14	0.15	0.17

The combined cycle relative contributions of all species to CO_2e emissions are shown in the SI. For the dual fuel tests on vehicle B, the next largest contributor was N_2O emissions with 10% and 16% of the CO_2 contribution for tests B1 and B2 respectively. Measured N_2O emissions for these tests were significantly higher than for B0 or for any of the tests with vehicle A Tailpipe NO_x emissions during the motorway phase of B1 were significantly increased compared to B0. This is despite post-turbo NO_x emissions being approximately halved in B1 compared to B0 over the same phase (shown in the SI). For vehicle A dual fuel tests, post-turbo NO_x emissions were reduced by ~40% and tailpipe NO_x by ~50% during the motorway phase compared to the baseline A0. For A1, post-turbo and tailpipe NO_x emissions were reduced by 30% compared to diesel over the combined cycle. Post-turbo NO_2/NO_x ratios were also different for dual fuel compared to diesel; for A1 this ratio was 0.34 over the combined cycle compared to 0.06 for A0 (shown in the SI). After the SCR, NO_2/NO_x ratios decreased to 0.15 for A1 and increased to 0.22 for A0. Indeed at the tailpipe, dual fuel NO_2/NO_x ratios are generally lower than for the diesel tests for both vehicles A and B. Performance of the SCR systems over the combined cycle reduced from 43% to 34-41% comparing A0 to A1 and A2, and 83% to 67% comparing B0 to B1. These results indicate that duel fuel operation affects the efficacy of the OEM SCR systems.

Particle mass and particle number emissions in warm start dual fuel tests were higher than the baseline diesel tests. The distance averaged particle size distributions (i.e. weighted by

exhaust volumetric flow and divided by cycle distance) are shown in Figure 1. Bimodal distributions are present for all tests. Comparing A1 to A0, the PM mass emissions factor is increased by ~30% due to a shift in the accumulation mode peak diameter from ~65 nm to ~85 nm with total particle number emissions approximately equivalent. The peak of the accumulation mode for vehicle B is not shifted significantly between B0 and B1, however the PN emissions are increased by ~20% leading to a ~30% increase in total PM mass. Cold start tests led to a more significant nucleation mode peaks and reduced accumulation mode peaks relative to equivalent hot start tests. The contribution of BC mass to CO_2e emissions as a percentage of the CO_2 contribution is between 1.8-4.3% for vehicle A and 0.5-1.3% for vehicle B relative to CO_2. BC mass contributed between 60-80% of total PM mass, across all transient tests, as shown in the SI along with uncertainties on the particle size distributions. Steady state PM mass emissions for vehicle A are discussed further in the following section.

Engine power specific emissions factors for vehicle A over the combined FIGE/ETC cycle are shown in the SI and compared to EURO V regulatory values for engine dynamometer tests over the equivalent cycle[28]. The baseline A0 configuration is compliant with CO and PM mass standards, however NO_x emissions are ~2.5 times higher than the standard (2.0 g/kWh). Indeed, NO_x emissions were higher than the EURO V standard for all vehicle A configurations. Dual fuel operation led to increased CO emissions for A1, however the oxidation catalyst on configuration A2 meant CO emissions were equal to those of A0. CH_4 emissions, which are only regulated for NG engines at type-approval[28], were 8.9 times higher than the regulatory limit value (1.1 g/kWh) for the A1 configuration of this aftermarket dual fuel system.

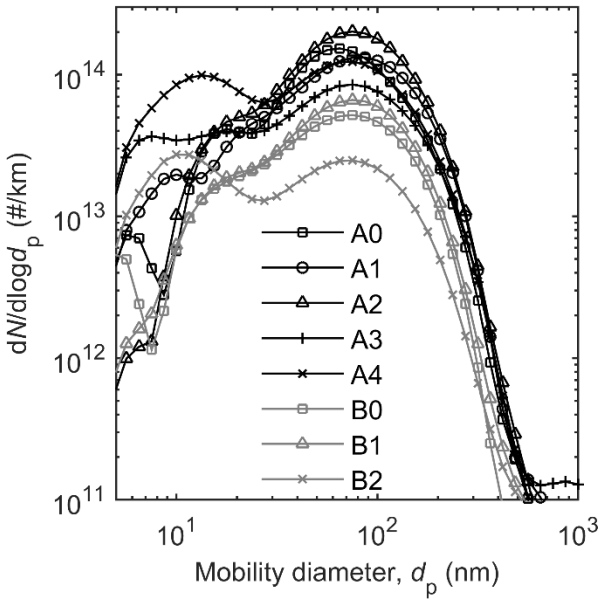

Figure 1: Distance specific particle size distributions over the combined FIGE cycle.

3.2 Steady state emissions

Steady state maps of ESR and CH_4 slip for A1, and the ratio of dual fuel to diesel (A1:A0) CO_2 and CO_2e emissions as a function of engine speed and torque are shown in Figure 2. For A1, the ESR reaches ~70% for engine speeds between 1200 and 1600 rpm and relatively low engine torque around ~300 Nm. At higher engine torque output and engine speeds, the ESR is reduced (as controlled by the system supplier's own proprietary software); at 600 Nm, the ESR is between 50-60% for the 1200-1600 rpm range. This can be cross referenced to the average ESR over the motorway phase of the transient cycle measured to be 58% for A1, during which the average engine torque and speed were approximately 600 Nm and 1400 rpm respectively. CH_4 slip is greatest at higher engine speeds, indicating that incomplete combustion of CH_4 is most significant when the in-cylinder residence time is lowest. The ratio of CO_2 emissions for A1 versus A0 indicates that the greatest reduction in CO_2 emissions is around 15% and that this occurs for engine speeds between 1000-1600 rpm and engine torque between 300-500 Nm. This corresponds to areas of high ESR (50-70%) and lower engine speeds. However, as shown for the transient cycle emissions, CH_4 emissions for A1 lead to higher total CO_2e emissions over almost the entire map compared to A0; this ratio is highest at low engine torques and higher engine speeds.

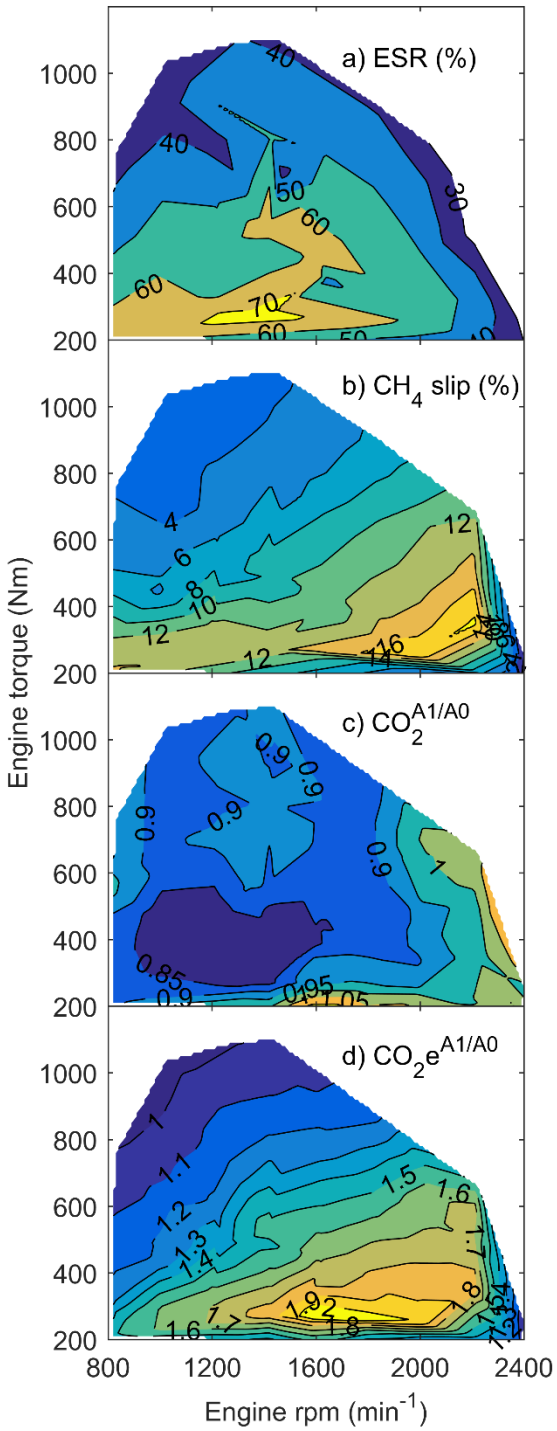

Figure 2: (a) Energy substitution ratio (ESR) of A1, (b) CH_4 slip of A1, (c) ratio of CO_2 emissions for A1:A0, and (d) ratio of CO_2e emissions for A1:A0 all as a function of engine speed and torque as measured during steady state testing of vehicle A.

Further evidence of incomplete combustion of CH_4 at higher engine speeds is provided in Figure 3, which shows the dual fuel to diesel (A1:A0) ratio of post-turbo NO_x and CO emissions and exhaust temperature. Dual fuel NO_x emissions are lower than diesel over most of the map, however the greatest reductions are observed for engine speeds greater than ~1800 rpm indicating lower average in-cylinder temperatures. This is further supported by the map of post-turbo exhaust temperatures which are generally lower for A1 than A0 for engine speeds greater than ~1800 rpm and engine torque greater than ~400 Nm. Post-turbo CO emissions, a product of incomplete combustion, are greater across the entire map for A1 compared to A0, and at high engine speeds they are increased by an order of magnitude.

Steady state PM mass emissions are shown in Figure 3 as a ratio of those measured for configurations A1 and A0. In the previous section, we showed that PM mass emissions increased for the dual fuel transient cycle tests compared to diesel. In Figure 3, it is evident that PM mass emissions are up to 50% lower for A1 compared to A0 at engine loads below 600 Nm and engine speeds below 2000 rpm. However at engine loads greater than 600 Nm and engine speeds less than 1500 rpm, PM mass emissions are increased for A1 compared to A0 by up to a factor of 3.

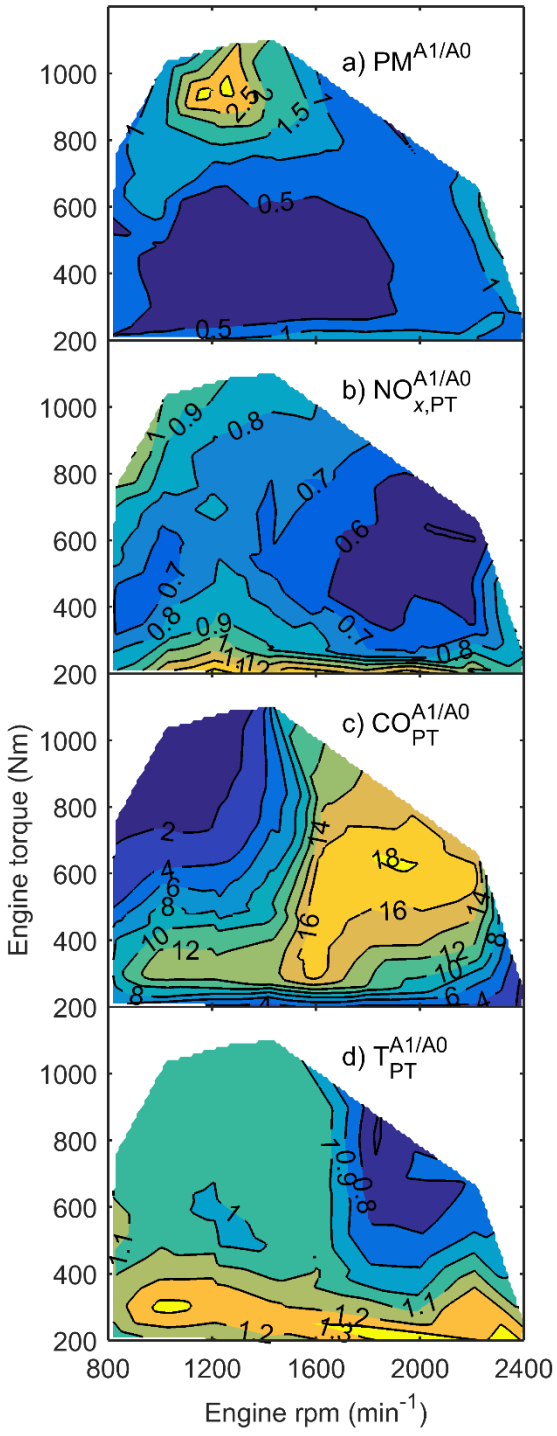

Figure 3: Ratios of (a) tailpipe PM mass emissions, (b) post-turbo (PT) NO_x emissions, (c) PT CO emissions, and (d) PT exhaust temperature as a function of engine speed and torque measured during steady state testing of vehicles A1 and A0.

3.3 Oxidation catalyst effectiveness

The effectiveness of the oxidation catalysts fitted to vehicles A2 and B1 during steady state testing is shown in Figure 4. The catalysed oxidation of CH_4 is a function of both residence time within the catalyst and exhaust gas temperature[37]. The measured catalyst effectiveness was greatest at high temperatures and residence times, i.e. low exhaust flow rates. For A2, the highest observed catalyst efficiency was 27% for a post-turbo exhaust temperature of 470°C and exhaust volumetric flow rate of 0.07 m^3/s. For B1, the highest observed catalyst efficiency was 30% for a post-turbo exhaust temperature of 505°C and exhaust volumetric flow rate of 0.10 m^3/s. For context, the average post-turbo exhaust temperatures and exhaust gas flow rates during the motorway phase of the transient cycle test were 396°C and 0.14 m^3/s for A2 and 370°C and 0.16 m^3/s for B1. These flow rates correspond to gas hourly space velocities of approximately 190,000 h^{-1} and 76,000 h^{-1} for the oxidation catalysts on A and B respectively. Below 400°C, the maximum performance of these catalysts were 15% and 10% for A2 and B1 respectively and therefore these results support the transient emissions results presented above that highlighted the significant contribution of tailpipe CH_4 to CO_2e emissions.

A benefit of the oxidation catalysts is to oxidise increased CO emissions during dual fuel operation to CO_2. Post-turbo and tailpipe CO emissions factors are shown in the SI. Even without the CH_4 oxidation catalyst, CO emissions are reduced by 72%, 81% and 76% by the SCR system for vehicles A0, A1 and A3 respectively. However, with the CH_4 oxidation catalyst, CO emissions are reduced by 94% and 92% for A2 and A4 respectively. Similarly, CO emissions were reduced by 95%, 93% and 97% for tests B0, B1 and B2 respectively.

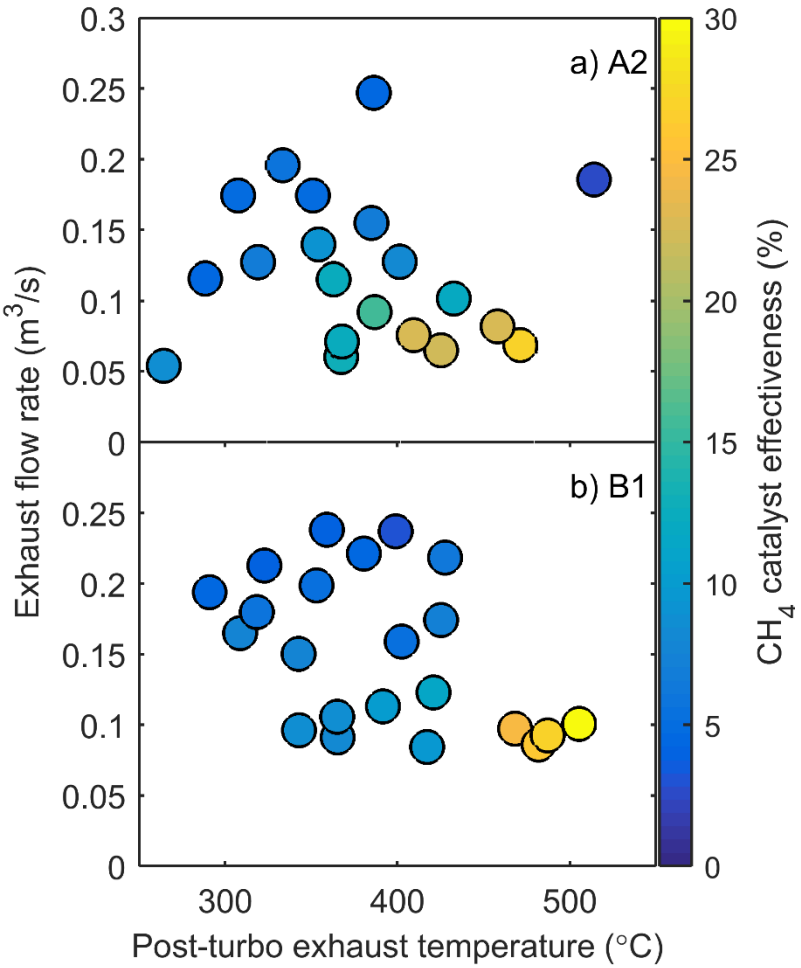

Figure 4: CH_4 oxidation efficiency of the catalyst present on (a) vehicle A2 and (b) B1 as a function of exhaust flow rate and post-turbo exhaust temperature as measured during steady state testing.

4 Discussion

This study evaluated the emissions performance of two vehicle platforms with five aftermarket dual fuel system configurations via chassis dynamometer testing of in-use vehicles that are part of trials of low-carbon trucks in the UK. All dual fuel systems evaluated in this study increased tailpipe total GHG (CO_2e) emissions compared to their equivalent diesel vehicles by 50% and 127% over the combined FIGE cycle for configurations A1 and B1 respectively. This is despite CO_2 emissions being reduced by up to ~9% and is primarily a result of incomplete combustion of CH_4 and subsequent CH_4 emissions, termed CH_4 slip. The three main mechanisms of CH_4 slip are (i) valve overlap which causes a proportion of the NG-air charge to be directly exhausted, (ii) incomplete combustion due to crevices and flame

quenching at the walls of the cylinder, and (iii) incomplete combustion due to lean NG-air mixtures and in-cylinder temperatures which prevent the flame from propagating throughout the charge.[21,38]Evidence for incomplete combustion and lower in-cylinder temperatures was provided by post-turbo emissions measurements showing higher CO and lower NO_x respectively at steady state conditions, especially at higher engine speeds when in-cylinder residence times are reduced. The results of this in-use vehicle emissions study are consistent with and supplement a large number of engine emissions studies showing that NO_x emissions decrease and CO emissions increase with dual fuel combustion relative to diesel. Thus, refinement of dual fuel systems to reduce CH_4 slip by addressing these three mechanisms and to improve CH_4 combustion efficiency are required. Our results suggests that reducing ESR at high engine speeds could have a beneficial effect on total CO_2e emissions and the magnitude of this effect over a transient drive cycle should be the topic of further modelling or experimental studies. Another example is to increase the diesel pilot quantity and advance the pilot injection timing[23], however trade-offs are increased NO_x emissions and lower ESR and therefore a reduced CO_2 benefit compared to diesel combustion. Direct CH_4 injection and stratification of the NG within the cylinder may also have the potential to reduce dual fuel CH_4 emissions.

CH_4 slip can also be controlled by exhaust after-treatment, however the oxidation catalysts tested in this study reduced CH_4 emissions by at most 15% at exhaust gas temperatures representative of transient conditions (~400°C). Thus, the commercial development of effective catalysts (e.g. Cargnello et al.[39]) that successfully oxidise CH_4 below 400°C are critical to the exploitation of NG as a transport fuel to reduce GHG emissions.

Both dual fuel platforms had higher PM mass emissions than their equivalent diesel configurations in transient testing. Steady state testing revealed that PM mass emissions were up to three times higher for dual fuel compared to diesel at high engine loads. While the majority of previous studies report decreases in PM mass emissions for dual fuel compared to diesel combustion[21], Papagiannakis et al.[40] reported an increase in soot opacity at high engine loads (80%) and ESR in the range of 30-50%. It is possible that this phenomena occurs due to the greater likelihood of rich combustion as a result of high diesel and NG flow rates during high engine load conditions. PM mass emissions were up to 50% lower at low engine loads, which is more consistent with existing literature and is attributable to the lower sooting tendency of premixed combustion of CH_4 compared to diffusion mode combustion of diesel[21].

Results for tailpipe NO_x emissions suggest that the change in exhaust gas composition in dual fuel operation could interfere with the efficacy of the OEM SCR system, which is optimised for diesel operation. Post-turbo and tailpipe exhaust gas temperatures (shown in the SI) are generally higher in the transient dual fuel tests compared to diesel, which may result from heat release via combustion of unburned hydrocarbons over the oxidation catalyst. At higher exhaust gas temperatures and higher NO_2/NO_x ratios the conditions in the SCR may be significantly different when the trucks are in dual fuel mode compared to diesel, thus affecting its performance[41]. Higher N_2O emissions for the dual fuel tests compared to diesel tests could be due to (i) higher rates of oxidation of ammonia to N_2O by NO_2 potentially caused by higher NO_2/NO_x ratios at temperatures up to 350°C[42], (ii) direct oxidation of ammonia by oxygen to N_2O at temperatures above 350°C[43] or (iii) by thermal decomposition of ammonium nitrate[44,45].

5 Acknowledgements

The authors would like to acknowledge support from the UK Engineering and Physical Sciences Research Council (EP/K00915X/1), the UK Department for Transport, the Office for Low Emission Vehicles and Innovate UK (project reference: 400266) and the industrial partners of the Centre for Sustainable Road Freight.

6 Supporting information

Additional details describing experimental methods, supplemental results and an uncertainty analysis are included in the Supporting Information (SI). This information is available free of charge via the Internet at http://pubs.acs.org.

7 Nomenclature

ρ_0	Material density (g/cm^3)
ρ_{eff}	Effective density (g/cm^3)
AR5	IPCC's Fourth Assessment Report
AR5	IPCC's Fifth Assessment Report
BC	Black carbon

C	Combined phases of FIGE drive-cycle
CO_2e	Carbon dioxide equivalent
D_m	Mass-mobility exponent
d_p	Particle mobility diameter (nm)
d_pp	Primary particle diameter (nm)
ESR	Energy substitution ratio (%)
ETC	European transient cycle developed by the FIGE institute
FTIR	Fourier transform infrared spectroscopy
GHG	Greenhouse gas
GWP	Global warming potential
HC	Unburned hydrocarbons
HGV	Heavy goods vehicle
HPDI	High-pressure direct injection
IPSD	Integrated particle size distribution
LCV	Lower (net) calorific value
LNG	Liquefied natural gas
M	Motorway (highway) phase of FIGE drive-cycle
$\dot{m}_{\mathrm{CH_4,in}}$	Mass flow rate of CH_4 supplied to the engine (kg/s)
$\dot{m}_{\mathrm{CH_4,tailpipe}}$	Mass flow rate of CH_4 exhausted at the tailpipe (kg/s)
$\dot{m}_{\mathrm{diesel,in}}$	Mass flow rate of diesel supplied to the engine (kg/s)
$\dot{m}_{\mathrm{NG,in}}$	Mass flow rate of natural gas supplied to the engine (kg/s)

NG	Natural gas
OEM	Original equipment manufacturer
PM	Particulate matter
PMP	Particle Measurement Programme
PN	Particle number
PT	Post-turbo (emissions sampling point)
U	Urban phase of FIGE drive-cycle
R	Rural phase of FIGE drive-cycle
rpm	Revolutions per minute
SCR	Selective catalytic reduction
T	Temperature (°C)

8 References

(1) International Energy Agency. *Energy Technology Perspectives 2012. Pathways to a Clean Energy System.*, 2nd ed.; IEA Publications: Paris, France, 2012.

(2) Department of Energy & Climate Change. Energy Consumption in the UK (ECUK) Transport data tables 2015 Update https://www.gov.uk/government/statistics/energy-consumption-in-the-uk (accessed Aug 6, 2015).

(3) Department of Energy & Climate Change. Final UK greenhouse gas emissions national statistics: 1990-2013 https://www.gov.uk/government/statistics/final-uk-emissions-estimates (accessed Aug 6, 2015).

(4) Ricardo-AEA. *Opportunities to overcome the barriers to uptake of low emission technologies for each commercial vehicle duty cycle*; London, UK, 2012.

(5) Atkins - Cenex. *Low Carbon Truck and Refuelling Infrastructure Demonstration Trial Evaluation. Second Annual Report to the DfT. Executive Summary for publication.*; 2015.

(6) European Commission. European Commission : CORDIS : Projects & Results Service : LNG-BC: Liquefied Natural Gas Blue Corridors http://cordis.europa.eu/project/rcn/198035_en.html (accessed Aug 6, 2015).

(7) US EPA. Alternative Fuel Conversion http://www.epa.gov/otaq/consumer/fuels/altfuels/altfuels.htm#4 (accessed Aug 6, 2015).

(8) Karim, G. A. A review of combustion processes in the dual fuel engine—The gas diesel engine. *Prog. Energy Combust. Sci.* **1980**, *6* (3), 277–285.

(9) Souto, J.; Ferrera, M.; Leclerq, N.; Matchett, M.; Magnusson, I. *LNG Blue Corridors: LNG Trucks Euro V technical solutions*; GC.SST.2012.2-3 GA No. 321592, 2014.

(10) Volvo Trucks. Volvo FM MethaneDiesel http://www.volvotrucks.com/trucks/global/en-gb/trucks/new-trucks/Pages/volvo-fm-methanediesel.aspx (accessed Jun 3, 2015).

(11) Prins Autogas UK Ltd. Prins Autogas UK: Dieselblend System http://www.prinsautogasuk.co.uk/dieselblend.php (accessed Jun 3, 2015).

(12) Clean Air Power. Clean Air Power: How it works http://www.cleanairpower.com/howitworks.html (accessed Jun 3, 2015).

(13) McTaggart-Cowan, G. P.; Bushe, W. K.; Hill, P. G.; Munshi, S. R. A supercharged heavy-duty diesel single-cylinder research engine for high-pressure direct injection of natural gas. *Int. J. Engine Res.* **2003**, *4* (4), 315–330.

(14) Karim, G. A. Combustion in Gas Fueled Compression: Ignition Engines of the Dual Fuel Type. *J. Eng. Gas Turbines Power* **2003**, *125* (3), 827.

(15) Stewart, J.; Clarke, A.; Chen, R. An experimental study of the dual-fuel performance of a small compression ignition diesel engine operating with three gaseous fuels. *Proc. Inst. Mech. Eng. Part D J. Automob. Eng.* **2007**, *221* (8), 943–956.

(16) Polk, A. C.; Gibson, C. M.; Shoemaker, N. T.; Srinivasan, K. K.; Krishnan, S. R. Detailed characterization of diesel-ignited propane and methane dual-fuel combustion in a turbocharged direct-injection diesel engine. *Proc. Inst. Mech. Eng. Part D J. Automob. Eng.* **2013**, *227* (9), 1255–1272.

(17) Gatts, T.; Liu, S.; Liew, C.; Ralston, B.; Bell, C.; Li, H. An experimental investigation of incomplete combustion of gaseous fuels of a heavy-duty diesel engine supplemented with hydrogen and natural gas. *Int. J. Hydrogen Energy* **2012**, *37* (9), 7848–7859.

(18) Besch, M. C.; Israel, J.; Thiruvengadam, A.; Kappanna, H.; Carder, D. Emissions Characterization from Different Technology Heavy-Duty Engines Retrofitted for CNG/Diesel Dual-Fuel Operation. *SAE Int. J. Engines* **2015**, *8* (3), 2015–01 – 1085.

(19) Papagiannakis, R. G.; Rakopoulos, C. D.; Hountalas, D. T.; Rakopoulos, D. C. Emission characteristics of high speed, dual fuel, compression ignition engine operating in a wide range of natural gas/diesel fuel proportions. *Fuel* **2010**, *89* (7), 1397–1406.

(20) Papagiannakis, R. G.; Hountalas, D. T. Combustion and exhaust emission characteristics of a dual fuel compression ignition engine operated with pilot Diesel fuel and natural gas. *Energy Convers. Manag.* **2004**, *45* (18-19), 2971–2987.

(21) Wei, L.; Geng, P. A review on natural gas/diesel dual fuel combustion, emissions and performance. *Fuel Process. Technol.* **2016**, *142*, 264–278.

(22) Rimmer, J. E.; Johnson, S. L.; Clarke, A. An experimental study into the effect of the pilot injection timing on the performance and emissions of a high-speed common-rail dual-fuel engine. *Proc. Inst. Mech. Eng. Part D J. Automob. Eng.* **2014**, *228* (8), 929–942.

(23) Sun, L.; Liu, Y.; Zeng, K.; Yang, R.; Hang, Z. Combustion performance and stability of a dual-fuel diesel-natural-gas engine. *Proc. Inst. Mech. Eng. Part D J. Automob.*

Eng. **2014**, *229* (2), 235–246.

(24) Gatts, T.; Liu, S.; Liew, C.; Ralston, B.; Bell, C.; Li, H. An experimental investigation of incomplete combustion of gaseous fuels of a heavy-duty diesel engine supplemented with hydrogen and natural gas. *Int. J. Hydrogen Energy* **2012**, *37* (9), 7848–7859.

(25) Graves, B.; Olfert, J.; Patychuk, B.; Dastanpour, R.; Rogak, S. Characterization of Particulate Matter Morphology and Volatility from a Compression-Ignition Natural-Gas Direct-Injection Engine. *Aerosol Sci. Technol.* **2015**, *49* (8), 589–598.

(26) Barlow, T. J.; Latham, S.; McCrae, I. S.; Boulter, P. G. *A reference book of driving cycles for use in the measurement of road vehicle emissions*; 2009.

(27) Hunt, S. W.; Odhams, A. M. C.; Roebuck, R. L.; Cebon, D. Parameter measurement for heavy-vehicle fuel consumption modelling. *Proc. Inst. Mech. Eng. Part D J. Automob. Eng.* **2011**, *225* (5), 567–589.

(28) European Union. *Directive 1999/96/EC of the European Parliament and of the Council of 13 December 1999 on the approximation of the laws of the Member States relating to measures to be taken against the emission of gaseous pollutants from positive ignition engines fuelled*; Official Journal of the European Communities L 44, 1999; p L 44/1 – L 44/155.

(29) United Nations Economic Commission for Europe (UNECE). *Global technical regulation No. 4. Test procedure for compression ignition (C.I.) engines and positive ignition (P.I.) engines fuelled with natural gas (NG) or liquefied petroleum gas (LPG) with regard to the emission of pollutants*; ECE/TRANS/180/Add.4, 2007.

(30) Maricq, M. M.; Xu, N. The effective density and fractal dimension of soot particles from premixed flames and motor vehicle exhaust. *J. Aerosol Sci.* **2004**, *35* (10), 1251–1274.

(31) Liu, Z. G.; Vasys, V. N.; Dettmann, M. E.; Schauer, J. J.; Kittelson, D. B.; Swanson, J. Comparison of Strategies for the Measurement of Mass Emissions from Diesel Engines Emitting Ultra-Low Levels of Particulate Matter. *Aerosol Sci. Technol.* **2009**, *43* (11), 1142–1152.

(32) Zheng, Z.; Durbin, T. D.; Xue, J.; Johnson, K. C.; Li, Y.; Hu, S.; Huai, T.; Ayala, A.; Kittelson, D. B.; Jung, H. S. Comparison of particle mass and solid particle number (SPN) emissions from a heavy-duty diesel vehicle under on-road driving conditions and a standard testing cycle. *Environ. Sci. Technol.* **2014**, *48* (3), 1779–1786.

(33) Mertes, S.; Schröder, F.; Wiedensohler, A. The Particle Detection Efficiency Curve of the TSI-3010 CPC as a Function of the Temperature Difference between Saturator and Condenser. *Aerosol Sci. Technol.* **1995**, *23* (2), 257–261.

(34) Giechaskiel, B.; Wang, X.; Horn, H.-G.; Spielvogel, J.; Gerhart, C.; Southgate, J.; Jing, L.; Kasper, M.; Drossinos, Y.; Krasenbrink, A. Calibration of Condensation Particle Counters for Legislated Vehicle Number Emission Measurements. *Aerosol Sci. Technol.* **2009**, *43* (12), 1164–1173.

(35) Giechaskiel, B.; Maricq, M.; Ntziachristos, L.; Dardiotis, C.; Wang, X.; Axmann, H.; Bergmann, A.; Schindler, W. Review of motor vehicle particulate emissions sampling and measurement: From smoke and filter mass to particle number. *J. Aerosol Sci.* **2014**, *67*, 48–86.

(36) Myhre, G.; Shindell, D.; Breon, F.-M.; Collins, W.; Fuglestvedt, J.; Huang, J.; Koch,

D.; Lamarque, J.-F.; Lee, D.; Mendoza, B.; et al. Anthropogenic and Natural Radiative Forcing. In *Climate Change 2013: The Physical Science Basis. Contribution of Working Group I to the Fifth Assessment Report of the Intergovernmental Panel on Climate Change.*; Stocker, T. F., Qin, D., Plattner, G.-K., Tignor, M., Allen, S. K., Boschung, J., Nauels, A., Xia, Y., Bex, V., Midgley, P. M., Eds.; Cambridge University Press: Cambridge, UK and New York, NY, USA, 2013.

(37) Gélin, P.; Primet, M. Complete oxidation of methane at low temperature over noble metal based catalysts: a review. *Appl. Catal. B Environ.* **2002**, *39* (1), 1–37.

(38) Dronniou, N.; Kashdan, J.; Lecointe, B.; Sauve, K.; Soleri, D. Optical Investigation of Dual-fuel CNG/Diesel Combustion Strategies to Reduce CO 2 Emissions. *SAE Int. J. Engines* **2014**, *7* (2), 873–887.

(39) Cargnello, M.; Delgado Jaén, J. J.; Hernández Garrido, J. C.; Bakhmutsky, K.; Montini, T.; Calvino Gámez, J. J.; Gorte, R. J.; Fornasiero, P. Exceptional activity for methane combustion over modular Pd@CeO2 subunits on functionalized Al2O3. *Science* **2012**, *337* (6095), 713–717.

(40) Papagiannakis, R. G.; Hountalas, D. T. Experimental investigation concerning the effect of natural gas percentage on performance and emissions of a DI dual fuel diesel engine. *Appl. Therm. Eng.* **2003**, *23* (3), 353–365.

(41) Koebel, M.; Elsener, M.; Kleemann, M. Urea-SCR: a promising technique to reduce NOx emissions from automotive diesel engines. *Catal. Today* **2000**, *59* (3-4), 335–345.

(42) Devadas, M.; Krocher, O.; Elsener, M.; Wokaun, A.; Soger, N.; Pfeifer, M.; Demel, Y.; Mussmass, L. Influence of NO2 on the selective catalytic reduction of NO with ammonia over Fe-ZSM5. *Appl. Catal. B Environ.* **2006**, *67* (3-4), 187–196.

(43) Madia, G.; Koebel, M.; Elsener, M.; Wokaun, A. Side Reactions in the Selective Catalytic Reduction of NO x with Various NO 2 Fractions. *Ind. Eng. Chem. Res.* **2002**, *41* (16), 4008–4015.

(44) Grossale, A.; Nova, I.; Tronconi, E.; Chatterjee, D.; Weibel, M. The chemistry of the NO/NO2–NH3 “fast” SCR reaction over Fe-ZSM5 investigated by transient reaction analysis. *J. Catal.* **2008**, *256* (2), 312–322.

(45) Grossale, A.; Nova, I.; Tronconi, E.; Chatterjee, D.; Weibel, M. NH3–NO/NO2 SCR for Diesel Exhausts Aftertreatment: Reactivity, Mechanism and Kinetic Modelling of Commercial Fe- and Cu-Promoted Zeolite Catalysts. *Top. Catal.* **2009**, *52* (13-20), 1837–1841.